Nuclear Inst. and Methods in Physics Research, A 1013 (2021) 165683

Contents lists available at ScienceDirect

Nuclear Inst. and Methods in Physics Research, A

journal homepage: www.elsevier.com/locate/nima

Electromagnetic calorimeters based on scintillating lead tungstate crystals for experiments at Jefferson Lab☆

A. Asaturyan [a], F. Barbosa [c], V. Berdnikov [b], E. Chudakov [c], J. Crafts [b,c], H. Egiyan [c], L. Gan [f], A. Gasparian [g], K. Harding [c], T. Horn [b], V. Kakoyan [a], H. Mkrtchyan [a], Z. Papandreou [e], V. Popov [c], N. Sandoval [c], A. Somov [c,*], S. Somov [d], A. Smith [h], C. Stanislav [c], S. Taylor [c], H. Voskanyan [a], T. Whitlatch [c], S. Worthington [c]

[a] A. I. Alikhanian National Science Laboratory (Yerevan Physics Institute), 0036 Yerevan, Armenia
[b] The Catholic University of America, Washington, DC 20064, USA
[c] Thomas Jefferson National Accelerator Facility, Newport News, VA 23606, USA
[d] National Research Nuclear University MEPhI, Moscow 115409, Russia
[e] University of Regina, Regina, Saskatchewan, Canada S4S 0A2
[f] University of North Carolina at Wilmington, Wilmington, NC 28403, USA
[g] North Carolina A&T State University, Greensboro, NC 27411, USA
[h] Duke University, Durham, NC 27708, USA

ARTICLE INFO

Keywords:
Electromagnetic calorimeter
Lead tungstate scintillator

ABSTRACT

A new electromagnetic calorimeter consisting of 140 lead tungstate ($PbWO_4$) scintillating crystals was constructed for the PrimEx-η experiment at Jefferson lab. The calorimeter was integrated into the data acquisition and trigger systems of the GlueX detector and used in the experiment to reconstruct Compton scattering events. The experiment started collecting data in the spring of 2019 and acquired about 30% of the required statistics. The calorimeter is a prototype for two $PbWO_4$-based detectors: the Neutral Particle Spectrometer (NPS) and the lead tungstate insert of the Forward CALorimeter (FCAL) of the GlueX detector. The article presents the design and performance of the Compton calorimeter and gives a brief overview of the FCAL and NPS projects.

1. Introduction

Electromagnetic calorimeters based on $PbWO_4$ scintillating crystals have a widespread application in experiments at different accelerator facilities such as CERN, FNAL, GSI, and Jefferson Lab (JLab) [1–5]. The small radiation length (L_R = 0.89 cm) and Molière radius (R_M = 2.19 cm) of $PbWO_4$ allows to build high-granularity radiation hard detectors with a good spatial separation and energy resolution of reconstructed electromagnetic showers, which makes these crystals the material of choice in many of these applications.

In this article we describe the design, construction, and performance of a calorimeter composed of 140 rectangular 2.05 cm × 2.05 cm × 20 cm $PbWO_4$ scintillating crystals, recently produced by Shanghai Institute of Ceramics (SICCAS). The calorimeter was used in the PrimEx-η experiment [6] with the GlueX detector [7] in the spring of 2019 to reconstruct Compton scattering events and is referred to as the Compton CALorimeter (CCAL).

The CCAL is a prototype for two large-scale $PbWO_4$-based detectors which are currently under construction in experimental Hall D and Hall C at Jefferson Lab: (1) the lead tungstate insert of the Forward CALorimeter (FCAL) of the GlueX detector and (2) the electromagnetic calorimeter of the Neutral Particle Spectrometer (NPS) [8]. The new calorimeters will be based on the $PbWO_4$ crystals of the same size as in the CCAL and use the same type of photodetectors and readout electronics. The crystals will be procured from two vendors: SICCAS in China and CRYTUR in the Czech Republic. $PbWO_4$ crystals are also being considered for an electromagnetic calorimeter of the future Electron–Ion Collider (EIC) [9].

* Corresponding author.
E-mail address: somov@jlab.org (A. Somov).

https://doi.org/10.1016/j.nima.2021.165683
Received 16 April 2021; Received in revised form 12 July 2021; Accepted 22 July 2021
Available online 24 July 2021

The lead tungstate insert of the FCAL consists of 1596 high-granularity, high resolution $PbWO_4$ crystals, which will be used to replace the lead glass modules in the inner part of the FCAL. This upgrade will improve the separation of showers and the shower energy resolution in the forward direction, which is required by the JLab Eta Factory (JEF) experiment to perform precision measurements of various $\eta^{(\prime)}$ decays with emphasis on rare neutral modes [10]. The design of the FCAL $PbWO_4$ module,[1] is based on that of the CCAL, except for some small modifications required to shield the magnetic field present in the calorimeter region. Studies of the magnetic shielding of photomultiplier tubes (PMT), and the design of the FCAL $PbWO_4$ module will be described in this article. The detector rates and operating conditions expected for the FCAL lead-tungstate insert were evaluated by using the CCAL during a few short GlueX physics runs at high luminosity. The measurements provided important information needed to optimize the design of the PMT divider and amplifier for GlueX run conditions.

The Neutral Particle Spectrometer [8] in experimental Hall C will consist of a $PbWO_4$ electromagnetic calorimeter preceded by a sweeping magnet. The NPS is required by Hall C's precision cross section measurement program with neutral final states [11–16]. Such precision measurements of small cross sections play a central role in studies of transverse spatial and momentum hadron structure. The NPS detector will consist of 1080 $PbWO_4$ crystals arranged in a 30×36 array.

Experience gained during fabrication and operation of the CCAL was critical for finalizing the design of the FCAL insert and also helped further optimize the NPS calorimeter. This article is organized as follows: we will present the PrimEx-η experiment and performance of the CCAL in Sections 2 and 3, and will briefly describe the FCAL and NPS projects in Sections 4 and 5.

2. PrimEx-η Experiment with the GlueX detector

The GlueX detector [7] was designed to perform experiments using a photon beam. Photons are produced via the bremsstrahlung process by electrons, provided by the JLab electron accelerator facility, incident on a thin radiator. The energy of a beam photon (E_γ) is determined by detecting a scattered electron after radiating the photon as follows: $E_\gamma = E_e - E'_e$, where E_e is the primary electron beam energy and E'_e is the energy of the bremsstrahlung electron. The bremsstrahlung electron is deflected in a 6 m long dipole magnet operated at a field of ~ 1.5 T and registered in the tagging scintillator counters. Each counter corresponds to the specific energy of the reconstructed electron. The tagging detectors span the beam photon energy range between 25% and 98% of the electron beam energy and cover the range between 2.8 GeV and 11.0 GeV during the PrimEx-η experiment.[2] The typical energy resolution of the beam photon is about 0.1%. The photon beam propagates toward the GlueX target. A schematic view of the GlueX detector is illustrated in Fig. 1.[3]

The physics goal of the PrimEx-η experiment is to perform a precision measurement of the $\eta \to \gamma\gamma$ decay width. The measurement will provide an important test of quantum chromodynamics symmetries and is essential for the determination of fundamental properties such as the ratios of the light quark masses and the η-η' mixing angle. The decay width will be extracted from the measurement of the photoproduction cross section of η mesons in the Coulomb field of a nucleus, which is known as the Primakoff effect. The η mesons will be reconstructed by detecting two decay photons in the forward calorimeter of the GlueX detector.

[1] The module consists of a $PbWO_4$ crystal wrapped with the light reflective foil and coupled to the photomultiplier tube with the divider.

[2] The electron beam energy during most production PrimEx-η runs was 11.2 GeV.

[3] Not shown on this plot is the DIRC detector, which was installed after the PrimEx-η experiment and is used for the particle identification in the forward direction.

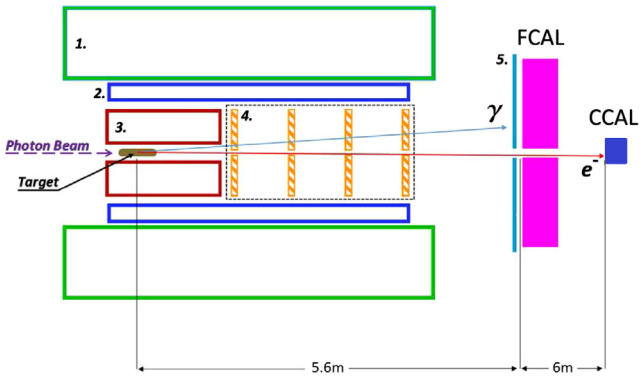

Fig. 1. Schematic layout of the GlueX detector (not to scale). Numbers represent the following detector components: solenoid magnet (1), barrel calorimeter (2), central drift chamber (3), forward drift chambers (4), time-of-flight wall (5).

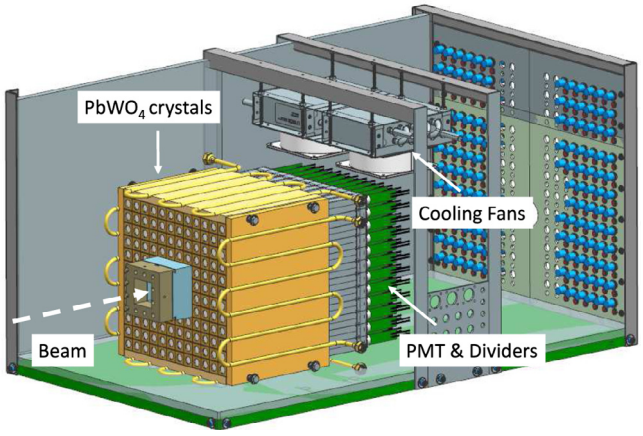

Fig. 2. Schematic layout of the Compton calorimeter.

The cross section will be normalized using the Compton scattering process, which will also be used to monitor the luminosity and control the detector stability during data taking. Electrons and photons originating from Compton events in the target are produced at small angles, typically outside the acceptance of the FCAL. In order to improve the particles reconstruction in the forward direction, we built a small Compton calorimeter consisting of 140 lead tungstate scintillating crystals. The CCAL was positioned about 6 m downstream from the FCAL as shown in Fig. 1. The CCAL covers the polar angle range θ between 0.19° to 0.47°.

The PrimEx-η experiment started collecting data in the spring of 2019 and has acquired 30% of the required statistics. During the experiment, the magnetic field of the solenoid magnet was switched off in order to allow reconstruction of Compton events. The photon flux was about $5 \cdot 10^6\ \gamma/\text{sec}$ (about five times lower than the nominal GlueX flux) in the beam energy range of interest between 9.5 GeV and 11.6 GeV.

3. Compton calorimeter of the PrimEx-η experiment

3.1. Calorimeter design

The calorimeter design is shown in Fig. 2. The CCAL comprises an array of 12×12 lead tungstate modules with a 2×2 hole in the middle for the passage of the photon beam. The modules are positioned inside a light tight box. A tungsten absorber is placed in front of the innermost layer closest to the beamline to provide protection from the high rate of particles predominantly originating from electromagnetic interactions.

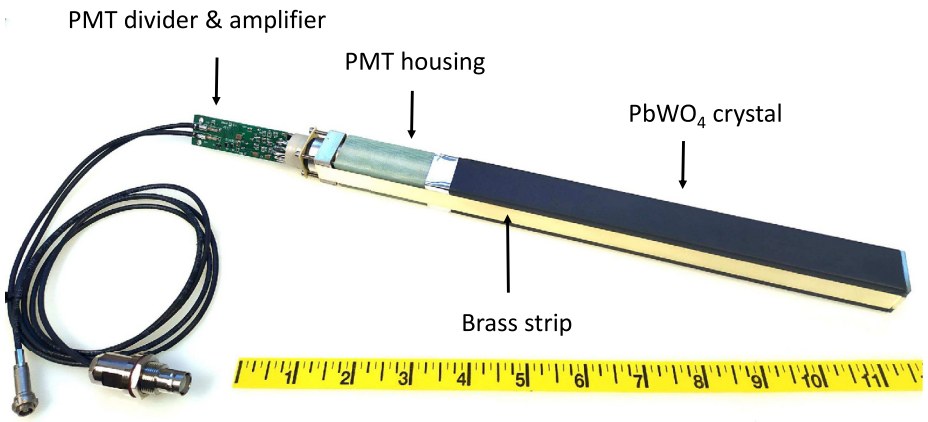

Fig. 3. Calorimeter module showing main components: the $PbWO_4$ crystal, PMT housing, PMT divider, and signal and high-voltage cables.

The light yield from $PbWO_4$ crystals depends on temperature and decreases at higher temperatures with a typical coefficient of 2%/°C at room temperature. Maintaining constant temperature is essential for the calorimeter operation. The calorimeter modules are surrounded by four copper plates with built-in pipes to circulate a cooling liquid and provide temperature stabilization. Foam insulation surrounds the detector box. In order to prevent condensation, a nitrogen purge is applied. Two fans with a water-based cooling system including radiators are installed on the top of the crystal assembly to improve nitrogen circulation and heat dissipation from the PMT dividers. The temperature was monitored and recorded during the experiment by five thermocouples attached to different points of the $PbWO_4$ module assembly. During the experiment the temperature was maintained at 17° ± 0.2 °C. The typical heat released by the photomultiplier tube dividers of the whole detector was equivalent to about 30 Watts. The detector was positioned on a platform, which allowed to move it in the vertical and horizontal directions, perpendicular to the beam. The platform was remotely controlled and provided a position accuracy of about 200 μm. During detector calibration each module was moved into the beam. The detector calibration will be discussed in Section 3.5.

3.2. Module design

The design of the $PbWO_4$ module is based on the HyCal calorimeter, which was used in several experiments in Jefferson Lab Hall B [17,18]. An assembled calorimeter module is presented in Fig. 3. Each lead tungstate crystal is wrapped with a 60 μm polymer Enhanced Specular Reflector film (ESR) manufactured by $3M^{TM}$, which allows 98.5% reflectivity across the visible spectrum. In order to improve optical isolation of each module from its neighbors, each crystal is wrapped with a layer of 25 μm thick Tedlar. The PMT is located inside a G-10 fiberglass housing at the rear end of the crystal. Two flanges are positioned at the crystal and housing ends and are connected together using 25 μm brass straps, which are brazed to the sides of the flanges. Four set screws are pressed to the PMT housing flange to generate tension in the straps and hold the assembly together. Light from the crystal is detected using a ten-stage Hamamatsu PMT 4125, which is inserted into the housing and is coupled to the crystal using optical grease (EJ-550) produced by Eljen Technology [19]. The PMT diameter is 19 mm. The PMT is pushed toward the crystal by using a G-10 retaining plate attached to the back of the PMT with four tension screws connected to the PMT flange. The PMT is instrumented with a high-voltage (HV) divider and amplifier positioned on the same printed circuit board attached to the PMT socket.

3.3. Electronics

The PMT of each calorimeter module are equipped with an active base prototype [20], which was designed for the Neutral Particle Spectrometer in experimental Hall C. The base combines a voltage divider and an amplifier powered by the current flowing through the divider. The active base allowed the operation of the PMT at lower voltage and consequently at lower anode current, which improves the detector rate capability and prolongs the PMT's life. The original Hamamatsu divider for this type of PMT was modified by adding two bipolar transistors on the last two dynodes, which provided gain stabilization at high rate. The active base had a relatively large amplification of about a factor of 24 due to the large PMT count rate predicted by Monte Carlo simulation of the NPS detector. Large amplification was not needed for the planned run conditions of the PrimEx-η experiment. However, we subsequently used CCAL in GlueX runs at significantly larger luminosity in order to study run conditions of the FCAL lead tungstate insert, where the amplifier will be required. This will be discussed in Section 4.0.3. During the PrimEx run, the CCAL PMTs were operated at about 680 V, which produced a divider current of 260 μA. The high voltage for each PMT was supplied by a 24-channel CAEN A7236SN module positioned in a SY4527 mainframe.

Amplified PMT signals were digitized using a twelve-bit 16-channel flash ADCs electronics module operated at a sampling rate of 250 MHz. The ADC was designed at Jefferson Lab [21] and is used for the readout of several sub-detectors of the GlueX detector. The Field-Programmable Gate Array (FPGA) chip inside the ADC module allows the implementation of various programmable data processing algorithms for the trigger and readout. An example of a flash ADC signal pulse obtained from a calorimeter module is shown in Fig. 4. In this example, the ADC was operated in the raw readout mode, where digitized amplitudes were read out for 100 samples, corresponding to the read out window size of 400 ns. During the PrimEx-η experiment, the ADC performed on-board integration of signal pulses, which amplitudes were above a threshold of 24 MeV. Amplitudes were summed in a time window of 64 ns and read out from the ADC module along with other parameters such as the pulse peak amplitude, pulse time, and data processing quality factors. This readout mode allowed to significantly reduce the data size and ADC readout time, and therefore did not induce any dead time in the data acquisition.

CCAL flash ADCs were positioned in a VXS (ANSI/VITA 41.0 standard) crate. VXS crates are used to host all readout electronics of the GlueX experiment. In addition to the VME-bus used to read out data from electronics modules, the VXS is instrumented with a high-speed serial bus in order to increase the bandwidth to several Gb/sec and provide an interconnected network between modules. The bus is used to transmit amplitudes digitized by the ADC to trigger electronics modules to include the CCAL in the Level 1 trigger system of the GlueX detector.

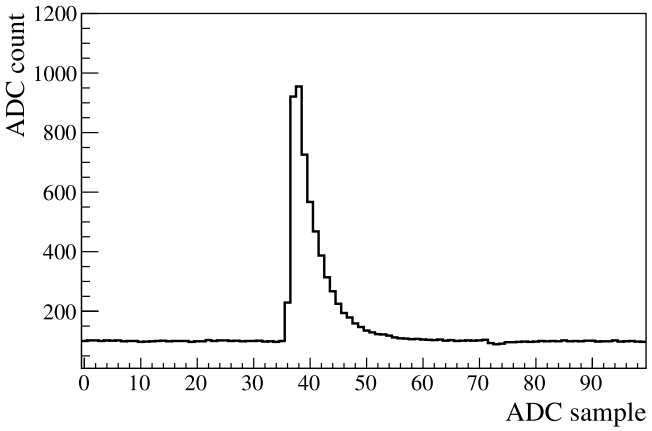

Fig. 4. A typical flash ADC signal pulse obtained from a $PbWO_4$ module.

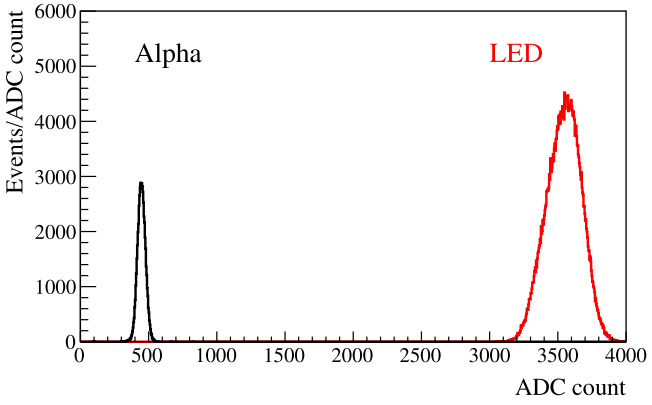

Fig. 5. Flash ADC signal amplitudes induced by the LED and α-source in the reference PMT.

3.4. Light monitoring system

To monitor performance of each calorimeter channel, we designed an LED-based light monitoring system (LMS). The LMS optics includes a blue LED, a spherical lens to correct the conical dispersion of the LED, and a diffusion grating to homogeneously mix the light. Light produced by the LED is incident on a bundle of plastic optical fibers (Edmund Optics) with a core diameter of 250 μm. Each fiber distributes light to an individual calorimeter module. On the crystal end, the fiber is attached to the module using a small acrylic cap glued to the crystal with a hole drilled through each cap to hold the fiber inside.

To monitor stability of the LED, we used two reference Hamamatsu 4125 PMTs, the same type as in the CCAL detector. Each PMT receives light from two sources: a single fiber from the LED and a YAP:Ce pulser unit, both glued to the PMT face. The pulser unit consists of a 0.15 mm thick YAP:Ce scintillation crystal with a diameter of 3 mm spot activated by an ^{241}Am α source. The α source is used to monitor stability of the LED. The PMT is read out using a flash ADC. The high voltage on each reference PMT is adjusted to have the signals from both the LED and α source fit within the range of a 12-bit flash ADC corresponding to 4096 counts, as shown in Fig. 5. Each LED is driven by a CAEN 1495 module, which allows to generate LED pulses with a programmable rate. The width of a signal pulse induced by the LED corresponds to about 80% of the pulse width produced by the $PbWO_4$ scintillating crystal. The typical amount of light injected by the LED to the crystal is equivalent to that emitted by 500 MeV photons.

The LMS was integrated into the GlueX trigger system and provided a special trigger type during data taking. The LMS was extensively used during the detector commissioning and injected light to the CCAL detector with a typical frequency of 100 Hz continuously during the PrimEx-η experiment. This LED rate was similar to the trigger rate of events produced by the reference α source.

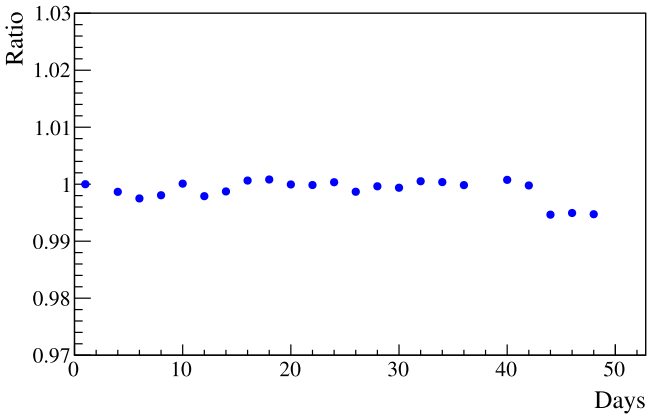

Fig. 6. Ratio of signal ADC amplitudes from the LED pulser to the α-source measured by the reference PMT during different run periods of the 48-day long PrimEx-η experiment. The ratio is normalized to data in the beginning of the run.

Most LMS components were positioned inside the temperature-stabilized detector box. The stability of the LED system measured using the reference PMTs during the entire PrimEx run was on the level of 1%. The ratio of signal ADC amplitudes from the LED pulser to the α source obtained during different run periods of the 48-day long PrimEx-η experiment is presented in Fig. 6. The ratio is normalized to the data in the beginning of the experiment. Stability of most CCAL modules observed using the LMS during about 1.5 months of the experiment was better than 6%. We did not apply any PMT gain adjustments during the experiment.

3.5. Calibration

The energy calibration of the CCAL was performed by moving the calorimeter platform and positioning each module into the photon beam during special low-intensity calibration runs; these were called snake scans. The maximum rate observed in the module exposed to the beam did not exceed 200 kHz at a threshold of 15 MeV. The energy of each beam photon was determined by detecting a bremsstrahlung electron using the GlueX tagging detectors described in Section 2. The tagging detectors covered the energy range of the photon beam between 2.8 GeV and 11 GeV. The spot size of the collimated beam had a diameter of about 6 mm.

The calibration procedure was organized into several steps. First, we adjusted HVs in the CCAL in order to equalize the energy response in the calorimeter modules for the given beam energy, and set the maximum signal pulse amplitude to the appropriate range of the flash ADC. We performed a snake scan, where the center of each module was sequentially placed into the beam. The signal pulse amplitudes were measured for that module. No shower reconstruction was done at this stage. An example of the signal amplitude in the calorimeter module in units of the flash ADC counts as a function of the beam energy is presented in Fig. 7. The PMT voltage was tuned to set the amplitude induced by 11 GeV photons to 3500 ADC counts (which corresponds to 1.7 V).

After adjusting voltages we repeated the snake scan and acquired data for the gain calibration. In the calibration we reconstructed showers in the calorimeter modules and constrained the reconstructed energy to the known beam energy. During shower reconstruction, energies from all modules constituting the shower were essentially summed up to the shower energy. For the CCAL shower reconstruction we adopted the algorithm which was originally used in the HyCal calorimeter [17] in JLab's experimental Hall B. The central part of the HyCal

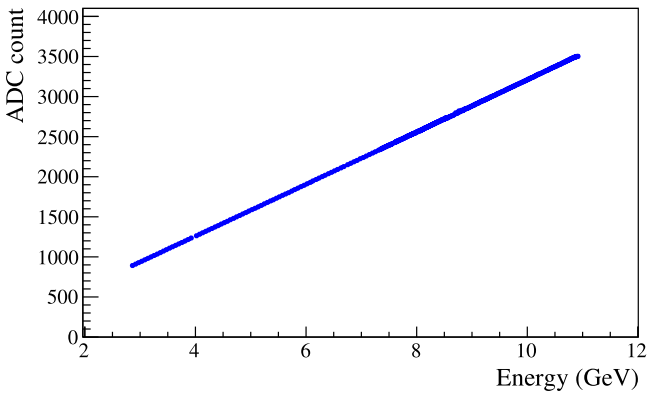

Fig. 7. ADC signal pulse amplitude in the CCAL module as a function of the beam energy.

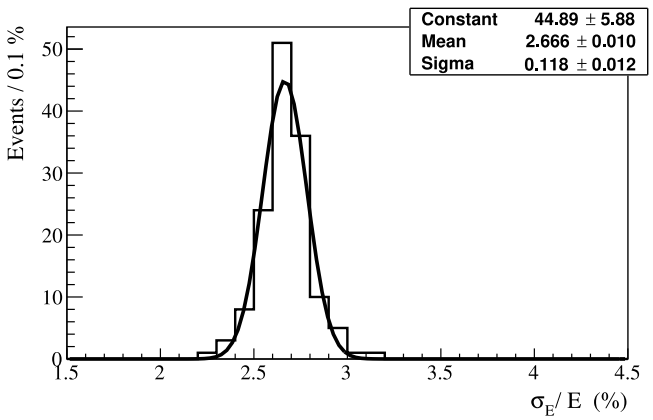

Fig. 8. Relative energy resolution of 140 $PbWO_4$ modules installed on the CCAL measured with 6 GeV beam photons.

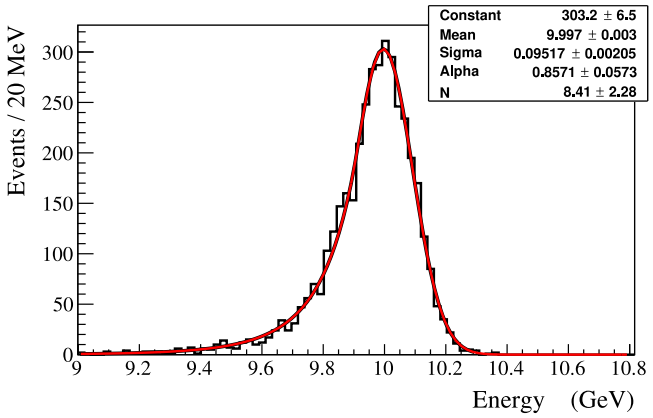

Fig. 9. Energy distribution deposited by 10 GeV beam photons. The spectrum is fit to a Crystal Ball function.

consists of the same type of crystals as those which we use in the CCAL. The gain of the central module in the shower, which was exposed to the beam was corrected as follows:

$$G_C = G_I \cdot \frac{E_{\text{Shower}}}{E_{\text{Beam}}}, \tag{1}$$

where G_I is the initial gain of the module before the correction, G_C is the corrected gain, E_{Shower} is the energy of the reconstructed electromagnetic shower, and E_{Beam} is the beam energy. For calibration, we used a constant beam energy of 4.5 GeV. The gain correction procedure was sequentially performed for all calorimeter modules, which were inserted into the beam. In order to account for shower leakage in the inner and outer layers of the calorimeter, the shower energy was adjusted in the reconstruction program. The energy leakage was computed and corrected for by using a shape of the shower profile. The calibration required a few iterations over all calorimeter modules.

The next step in the calibration was to determine corrections to the energy of reconstructed showers, which had to be applied in order to account for non-linear calorimeter responses due to readout energy thresholds, non linearity of the PMT and electronics, and shower leakage. In the CCAL reconstruction, the shower energy was corrected using a power function:

$$F(E) = P_0 \cdot E^{P_1+P_2\cdot E+P_3\cdot E^2}, \tag{2}$$

where E corresponds to the initial shower energy before the correction, and the constants, P, were obtained from the calibration. The shower energy correction was applied using calibration coefficients, P, corresponding to the shower module with the largest energy deposition. The parameters, P, were determined for each CCAL module individually using the snake scan data from a fit of the dependence of the reconstructed shower energy on the beam energy to the correction function in Eq. (2). The typical non-linear energy corrections to CCAL showers are 1–2% for the energies larger than 3 GeV, and 5–7% for 1 GeV showers. The relatively large correction required at small energies can be explained by a non-linear response of the PMT amplifier and the flash ADC readout threshold.

The CCAL calibration using the snake scans was performed in the beginning of the GlueX experiment. In order to account for some small drift of PMT gains on a level a few percent during the experiment, we adjusted the gains of the CCAL modules in data analysis using Compton scattering candidates. No corrections to the PMT's HVs were applied during data taking. In the calibration, we made use of the fact that the kinematics of the Compton scattering reaction is well defined. We selected showers in the CCAL produced by Compton candidates and computed the expected energy of an electron or photon, which initiated the shower, by using the shower's angle and known beam energy. The gain calibration procedure was similar to that described in the snake scan: the reconstructed and predicted energies of the shower were used to compute and apply gain corrections. We compared the energy resolution of reconstructed Compton candidates during different time periods of the PrimEx-η experiment, the difference was found to be smaller than 2%.

We estimated the non-uniformity of the 140 CCAL modules by measuring the relative energy resolution for each individual module exposed to the beam. As the beam can be positioned in the middle of each crystal with a good precision, better than 200 μm, the relative single-crystal energy resolution can characterize the uniformity of the crystals used in the calorimeter. We measured the energy deposited by 6 GeV photons in a single module and determined the energy resolution from a fit of the energy distribution to a Crystal Ball function [22]. The relative energy resolution, defined as the width of the energy distribution divided to the average energy deposited in the module, obtained for all 140 CCAL modules is presented in Fig. 8. The distribution is fit to a Gaussian function. The non-uniformity of the modules, i.e., the spread of the distribution is found to be smaller than 5%.

During calibration, we observed some non-linearity of the PMT active base with the large amplification factor of 24, on the level of a few percent, which impacted both the pulse peak and pulse integral. The base performance became linear when the amplifier gain was reduced. In order to study the impact of the non-linearity on the detector energy resolution, we replaced the original PMT active bases for 9 CCAL modules (in the array of 3×3 modules) with modified bases where the amplifier was bypassed. After adjusting high voltages and re-calibrating PMT gains, we measured the energy resolution for different beam energies. The beam was incident on the center of the middle module in the array. An example of the energy deposited by 10 GeV

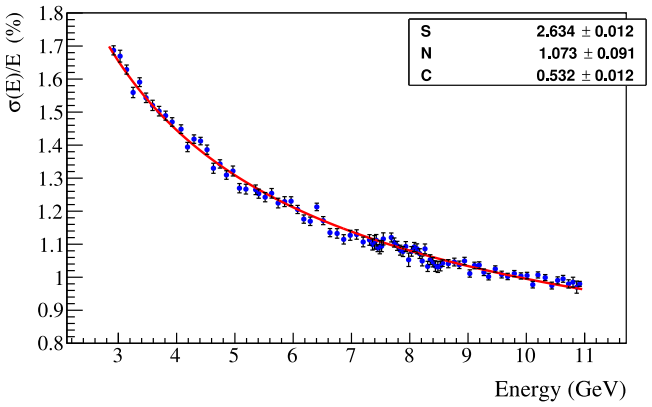

Fig. 10. The CCAL energy resolution as a function of the photon energy.

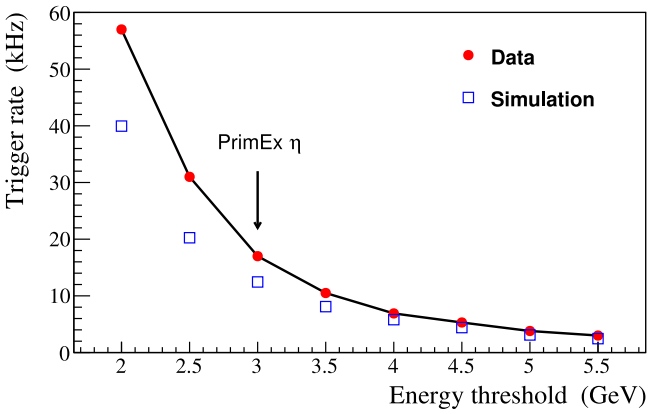

Fig. 11. Trigger rate as a function of the total energy deposited in the FCAL and CCAL. Circles represent data and boxes represent the rate of electromagnetic interactions predicted by Monte Carlo simulation. The arrow indicates the energy threshold used in PrimEx-η production runs.

photons is shown in Fig. 9. The energy resolution was obtained from a fit of the energy distribution to a Crystal Ball function[4] implemented in the ROOT data analysis framework [22]. The energy resolution as a function of the beam energy is shown in Fig. 10. The distribution was fit to the following function:

$$\frac{\sigma_E}{E} = \frac{S}{\sqrt{E}} \oplus \frac{N}{E} \oplus C, \tag{3}$$

where S represents the stochastic term, N the electronic noise and C the constant term, E is the beam energy in GeV, and the symbol $\oplus$ indicates a quadratic sum. The fit yields: $S = (2.63 \pm 0.01)\%$, $N = (1.07 \pm 0.09)\%$, and $C = (0.53 \pm 0.01)\%$. The resolution was found to be about 10% better than that measured with the original base with the amplifier gain factor of 24.[5] We note, that the energy resolution depends on the energy thresholds, and is getting worse with the increase of the readout threshold. This dependence is stronger at small shower energies. For the ADC readout threshold of 15 MeV per crystal used in the analysis the expected relative degradation of the energy resolution in our energy range of interest is small and constitutes to about 1.3% for 2.8 GeV showers and much smaller than a percent for the shower energies around 11 GeV. In the fit to the energy resolution, we did not account for the dependence on the readout threshold. The energy resolution decreases by 8% for 2.8 GeV photons if an energy threshold of 30 MeV is used. The energy resolution is consistent with that of the HyCal calorimeter [17], which was instrumented with crystals produced by SICCAS in 2001 and was used in several experiments in Jefferson Lab's experimental Hall B. The HyCal $PbWO_4$ crystals have the same transverse size of 2.05 cm × 2.05 cm, but a smaller length of 18 cm.

3.6. Performance during the PrimEx-η run

In the PrimEx-η experiment, we reconstructed Compton events produced by beam photons with the energy larger than 6 GeV. This energy range is covered by the GlueX pair spectrometer [23], which determines the photon flux needed for cross section measurements. An electron and photon produced in the Compton scattering process were detected by reconstructing two showers, one in the FCAL and another one in the CCAL. The event topology of the reaction is such that the more energetic electron predominantly goes into the Compton calorimeter, while the photon strikes the FCAL. In order to accept Compton events during data taking and to reduce background originating from low-energy electromagnetic and hadronic interactions, the CCAL was integrated to the Level 1 trigger system of the GlueX detector. The physics trigger was based on the total energy deposited in the forward and Compton calorimeters. The GlueX trigger is implemented on special-purpose programmable electronics modules with FPGA chips. The trigger architecture is described in Ref. [24]. The trigger rate as a function of the energy threshold is presented in Fig. 11. We collected data using a relatively small energy threshold of 3 GeV at a trigger rate of about 18 kHz. This rate did not produce any dead time in the data acquisition and trigger systems. The trigger rate is dominated by electromagnetic interactions, which was estimated using Geant detector simulation [25] and is superimposed on Fig. 11.

The typical rate in the CCAL modules measured during the experiment is presented in Fig. 12. In this plot, the photon beam goes through the center of the hole of 2 × 2 modules in the middle of the detector. The rate was the largest in innermost detector layers closest to the beamline. The maximum rate in the $PbWO_4$ crystal was about 200 kHz for an energy threshold of 30 MeV, which is equivalent to a signal pulse amplitude of 5 mV. This rate in the detector resulted in a negligibly small pile-up probability for the typical signal pulse width of 50 ns.[6] Before the experiment, we performed a high-rate performance study of the PMT and electronics using a laser and an LED periodic pulser and did not find any degradation of the PMT gain up to 2 MHz [26].

Timing resolution of reconstructed showers is an important characteristic of the detector performance. In the experiment we used timing information provided by the calorimeters to identify the accelerator beam bunch for which the interaction occurred in the detector and therefore related showers in the calorimeters with hits in the tagging detector, from the same event. A hit in the tagging detector defines the energy of the beam photon. The time in the calorimeter module is provided by an algorithm implemented on the programmable FPGA chip of the flash ADC. The algorithm performs a search of the peak of the signal pulse and determines the time from the shape of the leading edge of the pulse. The times of all hits constituting the CCAL shower are combined to form the shower time by using an energy-weighted sum. The time difference between beam photon candidates and CCAL showers originating from Compton events is presented in Fig. 13. The main peak on this plot corresponds to beam photons and CCAL clusters produced in the same accelerator bunch. Satellite peaks, separated by the beam bunch period of about 4 ns, represent accidental beam photons from accelerator bunches not associated with the interaction in the detector. The dependence of the time resolution, σ_t, of CCAL showers on the shower energy can be parameterized by the following

[4] The function is named after the Crystal Ball collaboration.

[5] The linearity of the PMT active base is being currently improved; modified active bases will be installed before the new PrimEx-η run in 2021.

[6] The pile-up effects can lead to the degradation of the energy resolution and have to be considered in the FCAL insert region closest to the beamline, where the rate will approach about 1 MHz per crystal.

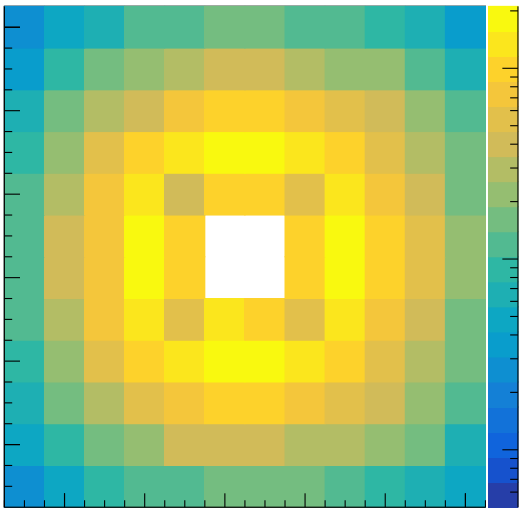

Fig. 12. Rates in the CCAL modules during PrimEx-η production run. The energy threshold corresponds to 30 MeV. The beam goes through the center of the hole in the middle of the plot.

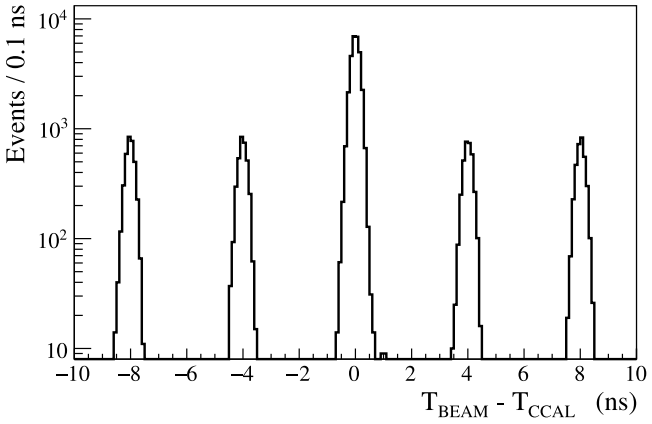

Fig. 13. Time difference between beam photons and reconstructed CCAL showers for Compton candidates. Peaks are separated by the beam bunch period of 4 ns.

function: $\sigma_t = \frac{0.32\text{ ns}}{\sqrt{E}} \oplus 0.09$ ns, where E is the shower energy in units of GeV, the symbol $\oplus$ denotes a quadratic sum, and the parameters were obtained from a fit to the data. The time resolution is improved with the increase of the shower energy and constitutes about 330 ps and 140 ps for 1 GeV and 9 GeV showers, respectively. In the PrimEx-η experiment the CCAL allowed a clear separation of beam photons originating from different beam bunches.

Reconstruction of electromagnetic showers in the FCAL is performed using an algorithm described in Ref. [27], which is a part of the standard GlueX reconstruction software. For the CCAL, we implemented an algorithm originally developed for the GAMS spectrometer [28, 29], which was subsequently adopted for the HyCal [17] in JLab's experimental Hall B. The algorithm was studied using Geant detector simulation [25]. No visible bias in the reconstructed shower energy was observed after applying a non-linear energy correction. The shower coordinates were reconstructed by combining the positions of all modules constituting the shower and using a logarithmically energy-weighted sum. The coordinates of a reconstructed shower exhibit a small bias on the level of 0.1–0.2 mm, which depends on the position of the incoming photon on the face of the crystal. The shower position resolution depends on the cluster energy and also correlates with the coordinate of the incident photon. The resolution is smaller near the edge of the crystal and increases at the crystal center. The typical position

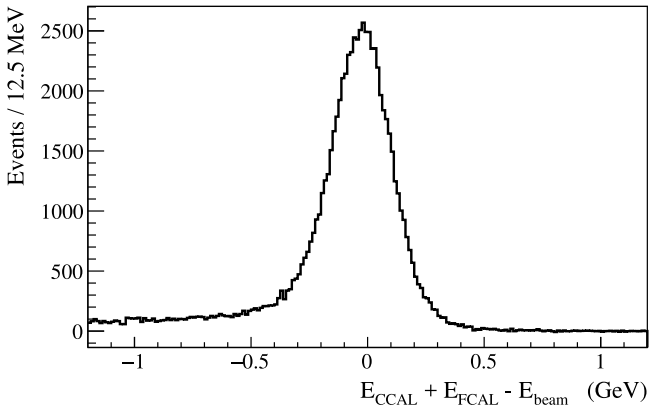

Fig. 14. Elasticity distribution of reconstructed Compton candidates. The elasticity is defined as the energy of two clusters in the calorimeters minus the beam energy.

resolution of 4 GeV photons is 1.4 mm. The algorithm provides a good separation of overlapping showers in the calorimeter by using profiles of electromagnetic showers. Two photons with energies between 1 GeV and 5 GeV positioned at a distance of 4 cm from each other can be reconstructed with a typical efficiency larger than 80%. The average shower multiplicity per event in the CCAL is ∼1.2. We consider to use this algorithm to reconstruct showers in the FCAL insert, which will be operated at significantly larger luminosity. In the reconstruction of Compton candidates we made use of the well defined kinematics of the two-body reaction. We selected events with two reconstructed showers, one in the CCAL and another one in the FCAL, that originated from the same beam interaction. The time difference between the showers and the beam photon was required to be smaller than 2 ns, which can be compared with the beam bunch period of 4 ns. We applied energy thresholds of 0.5 GeV and 1 GeV for showers reconstructed in the FCAL and CCAL, respectively. The difference in the azimuthal angle between the reconstructed photon and electron was required to be $|\Delta\phi| < 5\sigma_\phi$, where $\sigma_\phi = 5.5°$ is the angular resolution. For events that passed the selection criteria we used the elasticity distribution, which is defined as the reconstructed energy in the event minus the beam energy. The elasticity distribution for Compton candidates produced by beam photons in the energy range between 6 GeV and 7 GeV is presented in Fig. 14. The distribution was fit to the sum of a Gaussian and a second order polynomial function. The energy resolution of reconstructed Compton candidates in this energy range is 125 MeV. The measured resolution was found to be in a good agreement, at a level of a few percent, with that predicted by the Monte Carlo simulation. In this plot, we subtracted background originating from accidental beam photons. This background was measured using off-time interactions and amounted to about 15%. The relatively small background, on the level of 10%, produced by interactions of the photon beam with the beamline material downstream the GlueX target was measured using empty-target runs and was also excluded from the elasticity distribution in Fig. 14. The small remaining background under the peak of the elasticity distribution originates from the pair production reaction. For the beam energy range of interest, the e^+e^- pairs are typically produced at small polar angles. The pair production contribution was estimated using the Geant simulation to be on the level of a few percent. The CCAL allowed to clearly reconstruct Compton candidates in the PrimEx-η experiment.

4. Upgrade of the GlueX forward calorimeter

The forward calorimeter of the GlueX detector consists of 2800 lead glass modules, each with a size of 4 cm×4 cm×45 cm, and is positioned about 6 m downstream of the target, as shown in Fig. 1. The FCAL covers a polar angle of photons produced from the target between 1°

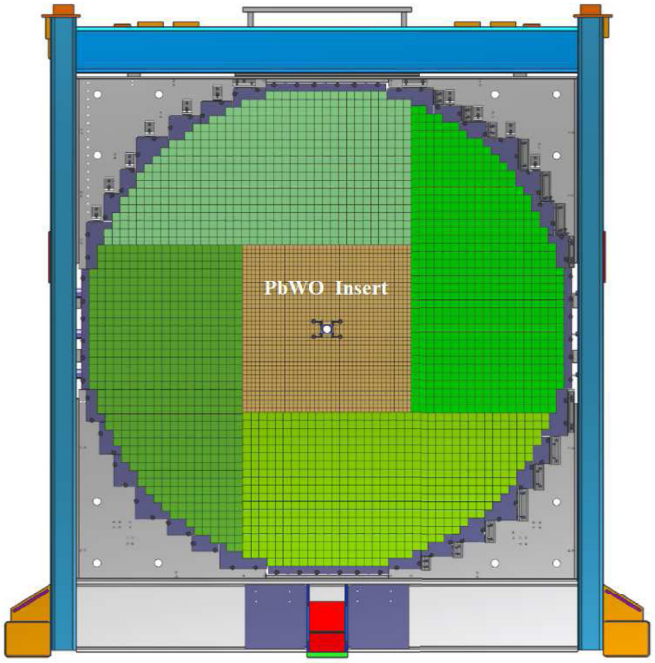

Fig. 15. FCAL frame with calorimeter modules installed: $PbWO_4$ crystals (brown area), lead glass blocks (green). The photon beam passes through the hole in the middle of the calorimeter. (For interpretation of the references to color in this figure legend, the reader is referred to the web version of this article.)

and 11° and detects showers with energies in the range of 0.1–8 GeV. The Cherenkov light produced in the module is detected by FEU-84-3 photomultiplier tubes, instrumented with Cockcroft–Walton bases [30]. The typical energy resolution of the FCAL is $\sigma_E/E = 6.2\%/\sqrt{E} \oplus 4.7\%$ [7].

The future physics program with the GlueX detector in Hall D will require an upgrade of the inner part of the forward calorimeter with high-granularity, high-resolution $PbWO_4$ crystals. The lead tungstate insert will improve the separation of clusters in the forward direction and the energy resolution of reconstructed photons by about a factor of two. Lead tungstate crystals possess better radiation hardness compared to lead glass, which is important for the long term operation of the detector at high luminosity. The size of the insert will tentatively comprise 1596 $PbWO_4$ crystals, which will form an array of 40×40 modules.[7] Similar to the CCAL, the insert will have a beam hole of 2×2 modules and a tungsten absorber used to shield the detector layer closest to the beamline. A schematic view of the FCAL frame with the installed lead tungstate insert is presented in Fig. 15. Due to the different size of the lead glass bars and lead tungstate crystals, the lead glass modules stacked around the $PbWO_4$ insert will form four regions with a relative offset between modules; those regions are shown in green color in this plot.

The $PbWO_4$ module design of the FCAL insert will essentially be the same as for the CCAL, except for some small modifications needed to handle the magnetic field present in the FCAL region. The PMT housing made of the G-10 fiberglass material will be replaced by a soft iron housing in order to reduce the magnetic field. The housing length will be increased to extend the magnetic shield beyond the PMT photocathode. An acrylic optical light guide will be inserted inside the PMT housing to couple the crystal and PMT.

The upgraded FCAL will be operated in GlueX experiments using a 30 cm long liquid hydrogen target at the designed photon flux of $5 \cdot 10^7$ γ/sec in the energy range between 8.4 GeV and 9 GeV. The designed luminosity is significantly larger than that used in the PrimEx-η experiment and was achieved after the PrimEx run in the fall of 2019.

[7] The insert size proposed for the JEF experiment [10] is 1 m × 1 m; the actual size will depend on the availability of funds.

In order to finalize the design of the PMT electronics, it is important to understand detector rates in the FCAL insert, especially in layers close to the beamline. We used the CCAL during high-intensity GlueX runs to study run conditions for the FCAL insert.

4.0.1. Magnetic shielding of PMTs

The longitudinal (directed along the beamline) and transverse (directed perpendicular to the axis of the beamline) components of the magnetic field produced by the GlueX solenoid magnet in the FCAL $PbWO_4$ insert area vary between 40–55 Gauss and 0–9 Gauss, respectively. The longitudinal field is the largest on the beamline, where the transverse component is practically absent. We studied the PMT magnetic shielding using a prototype consisting of an array of 3×3 PMT iron housings made of AISI 1020 steel, which was positioned in the middle of Helmholtz coils. Each housing had a size of 20.6 mm × 20.6 mm × 104 mm with a 20 mm round hole in the middle for the PMT. This corresponds to the realistic size of the magnetic shield that will be used in the calorimeter module assembly. Inside the housing we inserted two layers of mu-metal cylinders, with thicknesses of 350 μm and 50 μm, separated from each other by a Kapton film. The thickest cylinder was spot welded and annealed.

The Helmholtz coils had a diameter of about 1.5 m and can generate a uniform magnetic field with variable strength below 100 Gauss. A Hall probe was inserted into the central module of the prototype to measure the magnetic field at different Z-positions along the length of the cylinder. The field was measured for two different orientations of the prototype with respect to the magnetic field: field oriented along the PMT (longitudinal, B_z) and perpendicular to the PMT housing (transverse, B_x). Field measurements are presented in Fig. 16. The PMT shield significantly reduces both the longitudinal and transverse fields to the level of $B_z \sim 1$ Gauss and $B_x \ll 1$ Gauss. The transverse field, which is well shielded, is more critical for the PMT operation, as it is directed perpendicular to the electron trajectory inside the photo tube and deflects electrons, resulting in the degradation of the photon detector efficiency and gain. The field reaches a plateau at Z = 3 cm from the face of the housing. We will use a 3.5 cm long acrylic light guide in order to position the PMT in the area with the smallest magnetic field. The most sensitive to the magnetic field part of the PMT

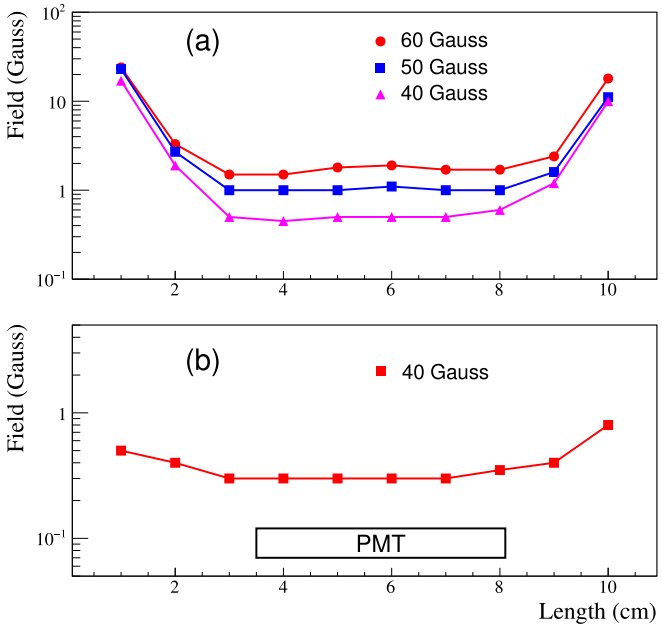

Fig. 16. Magnetic field distribution inside the PMT shield housing as a function of the distance from the housing face. Plot (a) corresponds to the longitudinal field and plot (b) corresponds to the transverse field produced by the Helmholtz coils. Markers denote different values of the magnetic field generated by the Helmholtz coils.

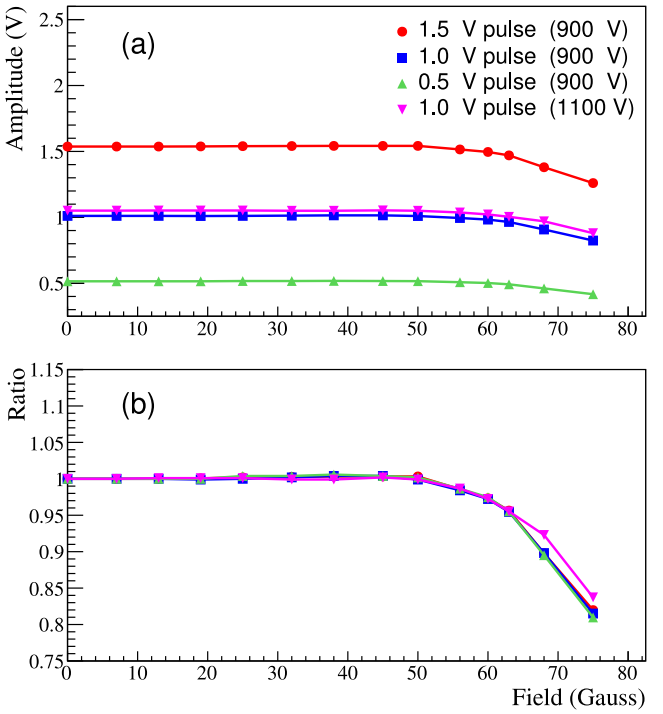

Fig. 17. Signal amplitudes of shielded PMT induced by an LED as a function of the magnetic field (a). Amplitudes, normalized to measurements without magnetic field (b). The PMT response was measured for different intensities of light pulse and HV settings as shown by different polymarkers.

is a 4.6 cm long region between the photocathode and the last dynode. The location of this region inside the PMT shield housing is shown as a box in Fig. 16. The actual field inside the FCAL insert module is expected to be even smaller due to the collective shielding effect, i.e., the large amount of shielding material installed on surrounding modules [31].

We studied performance of the shielded PMT in the magnetic field using an LED pulser. A blue LED with a light diffuser was placed about 20 cm from the PMT housing prototype and was aligned with the middle module. The PMT response was measured for different pulse amplitudes and operational high voltages. In order to study the contributions from longitudinal and transverse field components we rotated the prototype by different angles. Signal amplitudes as a function of the magnetic field measured in the prototype tilted by about 10 degrees are presented on the top plot of Fig. 17. Amplitudes, normalized to measurements without magnetic field, are shown on the bottom plot. The relative degradation of the signal amplitude for the maximum field in the FCAL insert region of B = 55 Gauss ($B_z \sim 54$ Gauss and $B_x \sim 9$ Gauss) was measured to be on the level of 1%. The proposed shielding configuration is sufficient to reduce the magnetic field to the level suitable for the PMT operation.

4.0.2. Light guide studies

Studies of the magnetic shielding demonstrated that the PMT has to be positioned inside the iron housing at the distance of at least 3 cm from the face of the $PbW0_4$ crystal. In order to do this, in the FCAL insert module we use a 3.5 cm long acrylic cylindrical light guide with a diameter of 18.5 mm between the PMT and the $PbWO_4$ crystal. The light guide is wrapped with reflective ESR foil and attached to the PMT with Dymax 3094 UV curing glue. Optical coupling to the crystal is provided by a "silicon cookie": a 1 mm thick transparent rubber cylinder made of the room temperature vulcanized silicon compound, RTV615. The silicon cookie is not glued to the light guide or the crystal, so the module can be easily disassembled if its PMT needs to be replaced.

We compared light losses of the FCAL insert module instrumented with the light guide with the CCAL module, where the PMT was coupled directly to the crystal using an optical grease. Light collection was measured using electrons provided by the Hall D pair spectrometer (PS) [23]. The PS is used to measure the flux of beam photons delivered to the experimental hall by detecting electromagnetic electron–positron pairs produced by the photons in a thin converter inserted to the beam. Leptons from the pair are deflected in a dipole magnet and registered using scintillator detectors placed in the electron and positron arms of the spectrometer. The energy of a lepton is detected using a high-granularity PS hodoscope, which consists of 145 scintillating tiles and covers the energy range between 3 GeV and 6 GeV. Each tile corresponds to the specific lepton energy.

The relative light yield of the module with and without the light guide was estimated by positioning the module behind the PS and measuring signal amplitudes induced by the PS electrons. We first measured the ADC response in the CCAL module, which was subsequently modified by adding the light guide to the same PMT and crystal and was placed to the same spot of the PS test setup. Results of the measurements are presented in Fig. 18. The ADC amplitude of the calorimeter module is presented as a function of the PS tile for the two module configurations with and without the light guide. The light guide results in a relatively small loss of light of $15 - 20\%$ compared with the CCAL module. We note that wrapping the light guide with the reflective material is important. Losses in unwrapped light guide constitute about 35%. We repeated light collection measurements using two more modules and obtained consistent results.

4.0.3. Detector rate

The PMT anode current is one of the critical characteristics that have to be considered during the design of the PMT divider. Typically the anode current should be on the level of a few micro amperes and significantly smaller than the divider current in order to provide stable performance of the PMT base and prevent the long-term degradation of the PMT. Some lifetime tests of the Hamamatsu 4125 PMT are described in Ref. [32].

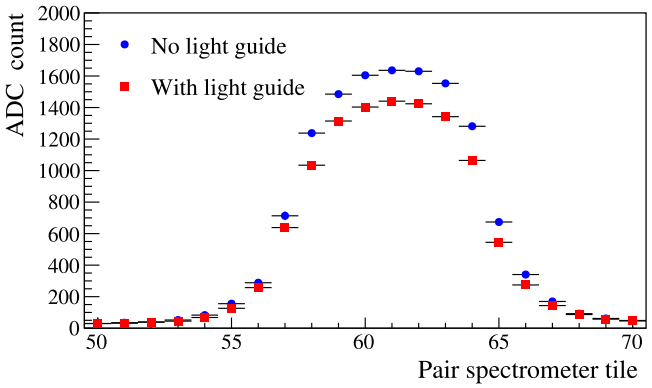

Fig. 18. ADC amplitudes of the calorimeter module as a function of the pair spectrometer tile for two configurations: the PMT directly coupled to the $PbWO_4$ crystal (circles), and the PMT coupled to the module using optical light guide (boxes).

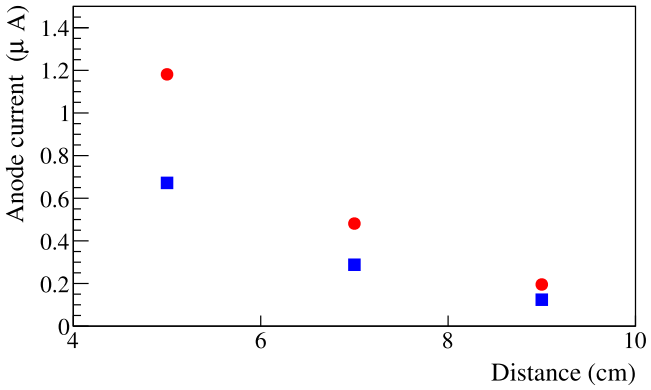

Fig. 19. Typical PMT anode current of CCAL modules positioned at different distances from the beamline. Circles correspond to the nominal GlueX luminosity, boxes correspond to 60% of the nominal luminosity.

The anode current (I) was measured in the CCAL modules during data production runs at the GlueX nominal luminosity. It was obtained by measuring the average voltage in the flash ADC induced by particles incident on the CCAL module as follows:

$$I = \frac{\bar{U}}{R} \cdot \frac{1}{G}, \tag{4}$$

where $\bar{U}$ is the average voltage in units of Volts, R is the input impedance of the amplifier ($\sim 50\ \Omega$), and G is the amplifier gain of 24. A periodic pulser not associated with an interaction in the detector was used as a trigger to read out flash ADC raw data for each CCAL module in a time window of 400 ns. The voltage was determined by summing up ADC amplitudes in the readout window and normalizing the sum to the window size. The typical anode current measured in CCAL modules situated at different distances from the beamline is presented in Fig. 19. Modules from the first CCAL layer closest to the beamline and the outer most layer were not used in the analysis. The inner modules were shielded by a tungsten absorber and the outer modules were obscured by the FCAL. The rate in the detector is dominated by the forward-directed electromagnetic background. The estimated anode current is the largest in the innermost layer of the detector closest to the beamline and amounts to about 1.4 μA. This current is significantly smaller than the PMT divider current of about 300 μA.

We used the CCAL measurements to estimate the current in the FCAL insert. Taking the geometrical location of FCAL and CCAL modules into account, the largest PMT current in the FCAL insert modules closest to the beamline and not shielded by the absorber was conservatively estimated to be about 15 μA. We assume that the PMT base is operated at 1 kV and no amplifier is used. The detector rate drops rapidly with the increase of the radial distance from the beamline. The estimated anode current is relatively large and must be reduced by lowering the PMT high voltage. We are considering to instrument PMTs in a few inner FCAL insert layers with an amplifier with a gain of 5 and to omit the amplifier on other modules. We are planning to perform more beam tests of the FCAL insert active base using the CCAL in forthcoming GlueX runs in 2021–2022.

5. Neutral particle spectrometer

The NPS is a new facility in Hall C that will allow access to precision measurements of small cross sections of reactions with neutral final states. The NPS consists of an electromagnetic calorimeter preceded by a sweeping magnet. As operated in Hall C, it replaces one of the focusing spectrometers.

The NPS science program currently features six fully approved experiments. E12-13-010 [11] and E12-06-114 [12] experiments will measure the Exclusive Deeply Virtual Compton Scattering and π^0 cross sections to the highest Q^2 accessible at Jefferson Lab. Both experiments will provide important information for understanding Generalized Parton Distributions (GPDs). The E12-13-007 [13] experiment will study semi-inclusive π^0 electroproduction process and seek to improve our understanding of the factorization framework, which is important for 12 GeV Jefferson Lab semi-inclusive deep-inelastic scattering program. Measurements of Wide-Angle and Timelike Compton Scattering reactions will be performed by the E12-14-003 [14] and E12-17-008 [15] experiments. These measurements will allow to test universality of GPDs using high-energy photon beams. The NPS will also be used in the E12-14-005 [16] experiment to study exclusive production of π^0 at large momentum transfers in the process $\gamma p \to \pi^0 p$.

The NPS science program requires neutral particle detection over an angular range between 6 and 57.3 degrees at distances of between 3 and 11 meters[8] from the experimental target. The experiments will use a high-intensity beam of electrons with the energies of 6.6, 8.8, and 11 GeV, and a typical luminosity of $\sim 10^{38}$ cm^{-2} s^{-1} as well as a secondary beam of photons incident on a liquid hydrogen target. A vertical-bend sweeping magnet with integrated field strength of 0.3 Tm will be installed in front of the spectrometer in order to suppress and eliminate background of charged particle tracks originating from the target. The photon detection is the limiting factor of the experiments. Exclusivity of the reaction is ensured by the missing mass technique and the missing-mass resolution is dominated by the energy resolution of the calorimeter. The calorimeter is anticipated to provide the spacial resolution of 2–3 mm and the energy resolution of about $2.5\%/\sqrt{E}$. The NPS consists of 1080 $PbWO_4$ crystals that form an array of 30×36 modules. Similarly to the FCAL insert in Hall D, the NPS will be built from the crystals of the same size, and instrumented with the same type of PMTs and readout electronics. The details of the mechanical assembly and commissioning of the NPS are currently under development and will be described in a forthcoming publication.

The radiation hardness and good optical quality of lead tungstate crystals are critical for the NPS calorimeter. The NPS collaboration, in a synergistic effort with the EIC eRD1 consortium, has characterized to date over 1200 $PbWO_4$ crystals produced by CRYTUR and SICCAS from 2014 to the present. The results of these studies have been published in Ref. [33]. CRYTUR crystal samples were found to have greater overall uniformity in transmittance and light yield, and better radiation hardness. Of the samples characterized by the NPS collaboration 140 SICCAS crystals have been used in the CCAL detector.

[8] The minimum NPS angle at 3 m is 8.5 degrees; at 4 m it is 6 degrees.

6. Summary

We described the design and performance of the Compton CALorimeter (CCAL), which was constructed using 140 lead tungstate $PbWO_4$ crystals recently produced by SICCAS. The calorimeter was successfully used in the PrimEx-η experiment in spring of 2019 for reconstruction of Compton scattering events. The CCAL served as a prototype for two large-scale electromagnetic calorimeters based on the $PbWO_4$ crystals: the lead tungstate insert of the Forward CALorimeter (FCAL) of the GlueX detector and the Neutral Particle Spectrometer (NPS). Experience gained during construction and operation of the CCAL provided important information for finalizing the design of FCAL $PbWO_4$ modules and understanding the performance of PMT dividers and also served to further optimize the NPS calorimeter. We anticipate to use the CCAL in forthcoming GlueX runs in 2021–2022 to perform final tests of the PMT dividers for the FCAL insert. We presented the design of the FCAL lead tungstate insert and gave an overview of the NPS project.

CRediT authorship contribution statement

A. Asaturyan: Conceptualization, Methodology. **F. Barbosa:** Conceptualization, Methodology, Supervision, Resources. **V. Berdnikov:** Conceptualization, Methodology, Formal analysis, Investigation, Software, Visualization, Writing – original draft. **E. Chudakov:** Conceptualization, Methodology, Supervision, Resources. **J. Crafts:** Conceptualization, Methodology, Investigation. **H. Egiyan:** Conceptualization, Methodology, Software. **L. Gan:** Conceptualization, Methodology, Investigation, Resources, Supervision, Project administration. **A. Gasparian:** Conceptualization, Methodology, Investigation, Supervision, Resources, Project administration. **K. Harding:** Conceptualization, Methodology. **T. Horn:** Conceptualization, Methodology, Supervision, Project administration, Funding acquisition, Resources, Writing – original draft. **V. Kakoyan:** Conceptualization, Methodology, Software. **H. Mkrtchyan:** Conceptualization, Methodology. **Z. Papandreou:** Conceptualization, Methodology, Supervision, Project administration, Resources, Writing – original draft. **V. Popov:** Conceptualization, Methodology. **N. Sandoval:** Conceptualization. **A. Somov:** Conceptualization, Methodology, Investigation, Formal analysis, Project administration, Supervision, Writing – original draft. **S. Somov:** Conceptualization, Methodology, Writing – original draft. **A. Smith:** Conceptualization, Software, Formal analysis. **C. Stanislav:** Conceptualization. **S. Taylor:** Conceptualization, Methodology, Formal analysis, Writing – original draft. **H. Voskanyan:** Conceptualization, Methodology. **T. Whitlatch:** Conceptualization, Methodology, Supervision, Resources. **S. Worthington:** Conceptualization, Methodology.

Declaration of competing interest

The authors declare that they have no known competing financial interests or personal relationships that could have appeared to influence the work reported in this paper.

Acknowledgments

This work was supported by the Department of Energy, USA. Jefferson Science Associates, LLC operated Thomas Jefferson National Accelerator Facility for the United States Department of Energy under contract DE-AC05-06OR23177. This work was supported in part by National Science Foundation, USA grants PHY-1714133, PHY-2012430 and PHY-1812396, and the U.S. Department of Energy Grant DE-FG02-03ER41231. We thank the NPS collaboration/project for providing $PbWO_4$ crystals and PMTs used in the construction of the CCAL.

References

[1] P. Adzic, et al., CMS Collaboration Collaboration, Results of the first performance tests of the CMS electromagnetic calorimeter, Eur. Phys. J. C 44S1 (2006) 1–10, http://dx.doi.org/10.1140/epjcd/s2005-02-011-3.
[2] D.D.V. Aleksandrov, et al., A high resolution electromagnetic calorimeter based on lead-tungstate crystals, Nucl. Instrum. Methods Phys. Res. A 550 (1) (2005) 169–184, http://dx.doi.org/10.1016/j.nima.2005.03.174.
[3] M. Kavatsyuk, et al., Performance of the prototype of the electromagnetic calorimeter for PANDA, Nucl. Instrum. Methods Phys. Res. A 648 (1) (2011) 77–91, http://dx.doi.org/10.1016/j.nima.2011.06.044.
[4] I. Balossino, et al., The HPS electromagnetic calorimeter, Nucl. Instrum. Methods Phys. Res. A 854 (2017) 89–99, http://dx.doi.org/10.1016/j.nima.2017.02.065.
[5] A. Acker, et al., The CLAS12 forward tagger, Nucl. Instrum. Methods Phys. Res. A 959 (2020) 163475, http://dx.doi.org/10.1016/j.nima.2020.163475.
[6] JLab Experiment E12-10-011, A Precision Measurement of the η Radiative Decay Width via the Primakoff Effect, available online: https://www.jlab.org/exp_prog/proposals/10/PR12-10-011.pdf.
[7] S. Adhikari, et al., GlueX Collaboration Collaboration, The GLUEX beamline and detector, Nucl. Instrum. Methods A 987 (2021) 164807, http://dx.doi.org/10.1016/j.nima.2020.164807, arXiv:2005.14272.
[8] Tanja Horn, JLab Neutral Particle Spectrometer Collaboration, A $PbWO_4$–based neutral particle spectrometer in Hall C at 12 GeV JLab, J. Phys. Conf. Ser. 587 (1) (2015) 012048, http://dx.doi.org/10.1088/1742-6596/587/1/012048.
[9] R. Abdul Khalek, et al., Science Requirements and Detector Concepts for the Electron-Ion Collider: EIC Yellow Report, 2021, arXiv:2103.05419.
[10] JLab Experiment E12-12-002, Eta Decays with Emphasis on Rare Neutral Modes: The JLab Eta Factory (JEF) Experiment, available online: https://www.jlab.org/exp_prog/proposals/14/PR12-14-004.pdf.
[11] JLab experiment E12-13-010, Exclusive Deeply Virtual Compton and Neutral Pion Cross-Section Measurements in Hall C, available online: https://www.jlab.org/exp_prog/proposals/13/PR12-13-010.pdf.
[12] JLab experiment E12-06-114, Measurements of the Electron-Helicity Dependent Cross Sections of Deeply Virtual Compton Scattering with CEBAF at 12 GeV, available online: https://www.jlab.org/exp_prog/proposals/06/PR12-06-114.pdf.
[13] JLab experiment E12-13-007, Measurement of SemiInclusive π^0 Production as Validation of Factorization, available online: https://www.jlab.org/exp_prog/proposals/13/PR12-13-007.pdf.
[14] JLab experiment E12-14-003, Wide-angle Compton Scattering at 8 and 10 GeV Photon Energies, available online: https://www.jlab.org/exp_prog/proposals/14/PR12-14-003.pdf.
[15] JLab experiment E12-17-008, Polarization Observables in Wide-Angle Compton Scattering at large s, t, and u, available online: https://www.jlab.org/exp_prog/proposals/17/PR12-17-008.pdf.
[16] JLab experiment E12-14-005, Wide Angle, Exclusive Photoproduction of π^0 Mesons, available online: https://www.jlab.org/exp_prog/proposals/14/PR12-14-005.pdf.
[17] M. Kubantsev, I. Larin, A. Gasparian, PrimEx Collaboration Collaboration, Performance of the primex electromagnetic calorimeter, in: S.R. Magill, R. Yoshida (Eds.), AIP Conf. Proc. 867 (1) (2006) 51–58, http://dx.doi.org/10.1063/1.2396938, arXiv:physics/0609201.
[18] A. Gasparian, PrimEx Collaboration Collaboration, A high performance hybrid electromagnetic calorimeter at jefferson lab, in: 11th International Conference on Calorimetry in High-Energy Physics (Calor 2004), 2004.
[19] Eljen Technology, Organic Scintillators, available online: https://eljentechnology.com.
[20] V. Popov, H. Mkrtchyan, New photomultiplier active base for hall c jefferson lab lead tungstate calorimeter, in: 2012 IEEE Nuclear Science Symposium and Medical Imaging Conference Record (NSS/MIC), 2012, pp. 1177–1179, http://dx.doi.org/10.1109/NSSMIC.2012.6551294.
[21] F. Barbosa, et al., A VME64x, 16-Channel, Pipelined 250 MSPS Flash ADC With Switched Serial (VXS) Extension, Tech. rep., Jefferson Lab, 2007, Technical Report GlueX-doc-1022 (hyperlink).
[22] R. Brun, F. Rademakers, ROOT: An object oriented data analysis framework, in: M. Werlen, D. Perret-Gallix (Eds.), Nucl. Instrum. Methods A 389 (1997) 81–86, http://dx.doi.org/10.1016/S0168-9002(97)00048-X.
[23] F. Barbosa, C. Hutton, A. Sitnikov, A. Somov, S. Somov, I. Tolstukhin, Pair spectrometer hodoscope for Hall D at Jefferson Lab, Nucl. Instrum. Methods A 795 (2015) 376–380, http://dx.doi.org/10.1016/j.nima.2015.06.012.
[24] A. Somov, JLab Fast Electronics Group Collaboration Collaboration GlueX, Development of level-1 triggers for experiments at jefferson lab, in: Bonnie Fleming (Ed.), AIP Conf. Proc. 1560 (1) (2013) 700–702, http://dx.doi.org/10.1063/1.4826876.
[25] J. Allison, et al., Recent developments in Geant4, Nucl. Instrum. Methods Phys. Res. A 835 (2016) 186–225, http://dx.doi.org/10.1016/j.nima.2016.06.125.
[26] F. Barbosa, et al., Characterization of the NPS and CCAL readout, Tech. rep., Jefferson Lab, GlueX-doc-3272, 2017, https://halldweb.jlab.org/doc-public/DocDB/ShowDocument?docid=3272.
[27] R.T. Jones, et al., A bootstrap method for gain calibration and resolution determination of a lead-glass calorimeter, Nucl. Instrum. Methods A 566 (2006) 366–374, http://dx.doi.org/10.1016/j.nima.2006.07.061.

[28] A. Lednev, Separation of the overlapping electromagnetic showers in the cellular gams-type calorimeters, Tech. rep., IHEP Protvino, 1993, pp. 93–153, Preprint IHEP.

[29] F. Binon, et al., Hodoscope multi-photon spectrometer GAMS-2000, Nucl. Instrum. Methods A 248 (1986) 86, http://dx.doi.org/10.1016/0168-9002(86)90501-2.

[30] A. Brunner, et al., A Cockcroft-Walton base for the FEU84-3 photomultiplier tube, Nucl. Instrum. Methods A 414 (1998) 466–476, http://dx.doi.org/10.1016/S0168-9002(98)00651-2.

[31] O. Glamazdin, TOSCA simulation of the magnetic shielding of the FCAL insert, Tech. rep., GlueX-doc-3561, Jefferson Lab, 2018, https://halldweb.jlab.org/doc-private/DocDB/ShowDocument?docid=3561.

[32] W. Koska, S.W. Delchamps, J. Freeman, W. Kinney, D. Lewis, P. Limon, J. Strait, I. Fiori, M. Gallinaro, Q. Shen, Evaluation of candidate photomultiplier tubes for the upgrade of the CDF end plug calorimeter, Nucl. Instrum. Methods A 406 (1998) 103–116, http://dx.doi.org/10.1016/S0168-9002(97)01193-5.

[33] T. Horn, et al., Scintillating crystals for the Neutral Particle Spectrometer in Hall C at JLab, Nucl. Instrum. Methods A 956 (2020) 163375, http://dx.doi.org/10.1016/j.nima.2019.163375, arXiv:1911.11577.